JOURNAL OF SOLID STATE CHEMISTRY 77, 336–341 (1988)

X-Ray Photoelectron Spectroscopy Study of $(Nd_{1-x}Ca_x)MnO_{2.99}$ $(0.5 \leqq x \leqq 1.0)$

H. TAGUCHI* AND M. NAGAO

Research Laboratory for Surface Science, Faculty of Science, Okayama University, Okayama 700, Japan

M. SHIMADA

Department of Applied Chemistry, Faculty of Engineering, Tohoku University, Sendai 980, Japan

AND Y. TAKEDA AND O. YAMAMOTO

Department of Chemistry, Faculty of Engineering, Mie University, Tsu 514, Japan

Received April 12, 1988; in revised form July 20, 1988

The X-ray photoelectron spectroscopy of perovskite-type $(Nd_{1-x}Ca_x)MnO_{2.99}$ $(0.5 \leqq x \leqq 1.0)$ was measured at room temperature. The integrated intensity of Nd4*d* linearly decreases and that of Ca2*p* linearly increases with increasing x. The binding energies of Nd4*d*, Ca2*p*, and O1*s* decrease with increasing x. On the other hand, both the integrated intensity and the binding energy of Mn2*p* are independent of the composition. The electron transfer of the Mn–O–Mn path is dominant in the Ca-poor region. With increasing x, the electron transfer of the Mn–O–(Nd,Ca)–O–Mn path also occurs. However, in the high Ca-rich region, the high electronegativity of Ca prevents the electron transfer of the Mn–O–(Nd,Ca)–O–Mn path.

Introduction

$(Nd_{1-x}Ca_x)MnO_{2.99}$ has the orthorhombic perovskite-type structure and exhibits *n*-type semiconductor at low temperature in the range $0.5 \leqq x \leqq 0.9$ (*1*). The electrical resistivity of $(Nd_{1-x}Ca_x)MnO_{2.99}$ decreases with increasing x and reaches a minimum value at ca. $x = 0.9$, and then abruptly increases in analogy with $(La_{1-x}Ca_x)MnO_{2.97}$ (*2*). In the semiconductor region, the electrical resistivity follows the Mott's $T^{-1/4}$ law indicating the possible occurrence of variable range hopping of electrons due to Anderson localization (*3*, *4*).

At high temperature, $(Nd_{1-x}Ca_x)MnO_{2.99}$ exhibits a metal–insulator transition. From the results of DTA and DSC measurements, the metal–insulator transition occurs without the crystallographic change. On the other hand, the magnetic susceptibility has a deflection point near the metal–insulator transition temperature. From the results of the electrical, magnetic, DTA,

* To whom all correspondence should be addressed.

0022-4596/88 $3.00

and DSC measurements, the mechanism of the metal–insulator transition in $(Nd_{1-x}Ca_x)MnO_{2.99}$ is explained by the band model proposed by Goodenough (*5*).

X-ray photoelectron spectroscopy (XPS) of perovskite-type $CaMnO_{3-\delta}$ and $(La_{1-x}Ca_x)MnO_{2.97}$ was measured at room temperature by Taguchi and Shimada (*6*, *7*). In $CaMnO_{3-\delta}$, the binding energy of Ca2*p* decreases with decreasing oxygen content, but the binding energy of O1*s* increases with decreasing oxygen content. On the other hand, the binding energy of Mn2*p* is independent of the oxygen content. In $(La_{1-x}Ca_x)MnO_{2.99}$, the binding energies of La3*d*, Ca2*p*, and O1*s* decrease with increasing x, but the binding energy of Mn2*p* is independent of the composition.

In the present study, XPS of $(Nd_{1-x}Ca_x)MnO_{2.99}$ ($0.5 \leqq x \leqq 1.0$) is measured at room temperature to examine the partial ionic character of Ca, Nd, Mn, and O. These results will provide information on the electrical properties corresponding to the electron transfer of the Mn–O–Mn path and the Mn–O–(Nd,Ca)–O–Mn path in the perovskite-type manganates.

Experimental

Samples were prepared using a standard ceramic technique. Powders of Nd_2O_3, $CaCO_3$, and $MnCO_3$ were weighed in the desired proportions and milled for a few hours with acetone. After the mixed powders were dried at 373 K, they were calcined in air at 1073 K for 24 hr, then fired at 1623 K for 24 hr under a stream of pure oxygen gas. The oxygen-deficient materials obtained in this way were annealed at 873–973 K under a stream of pure oxygen gas for 24 hr.

The phases of the samples were identified by X-ray powder diffraction with filtered Cu$K\alpha$ radiation. The oxygen content of each sample was determined by the oxidation-reduction method (*8*). XPS measurements were carried out for Nd4*d*, Ca2*p*, Mn2*p*, and O1*s* levels of the samples using Mg$K\alpha$ radiation ($h\nu$ = 1254.6 eV) at room temperature. The energy calibration was made against the Au4$f_{7/2}$ peak, which was sputtered on the samples.

Results and Discussion

X-ray powder diffraction patterns of all samples were completely indexed as the orthorhombic perovskite-type structure. The oxygen contents of all samples annealed at 873–973 K in a stream of pure oxygen gas were determined to be 2.99 (δ = 0.01) from the chemical analysis.

Figure 1 shows the XPS spectra of the Nd4*d* level. The Nd4*d* peak is broad, and the integrated intensity of the Nd4*d* peak linearly decreases with increasing x. Figure 2 shows the XPS spectra of the Ca2*p* level. The Ca2$p_{1/2}$ and Ca2$p_{3/2}$ peaks are sharp, and the integrated intensities of the Ca2$p_{1/2}$

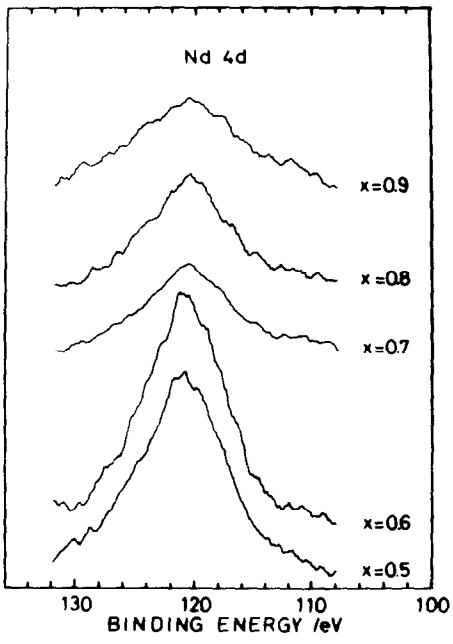

FIG. 1. XPS spectra of the Nd4*d* level in the system $(Nd_{1-x}Ca_x)MnO_{2.99}$.

and Ca2$p_{3/2}$ peaks linearly increase with increasing x. In Fig. 2, the peak of ca. 353 eV is assigned to Au4$d_{3/2}$ sputtered on the sample. The satellite peaks on the high binding energy side of the Ca2p peaks are separated from the main peaks by ca. 1.0 eV, and this value is independent of the composition. In $(La_{1-x}Ca_x)MnO_{2.97}$, the energy difference between the Ca2p peak and the satellite peak is ca. 1.2 eV, which is also independent of the composition (*7*). On the other hand, in $CaMnO_{3-\delta}$, the energy difference between the Ca2p peak and the satellite peak increases from ca. 1.2 eV to ca. 2.0 eV with decreasing oxygen content (*6*). From these results, the energy difference between the Ca2p peak and the satellite peak is considered to be strongly influenced by the oxygen content in the perovskite-type manganates.

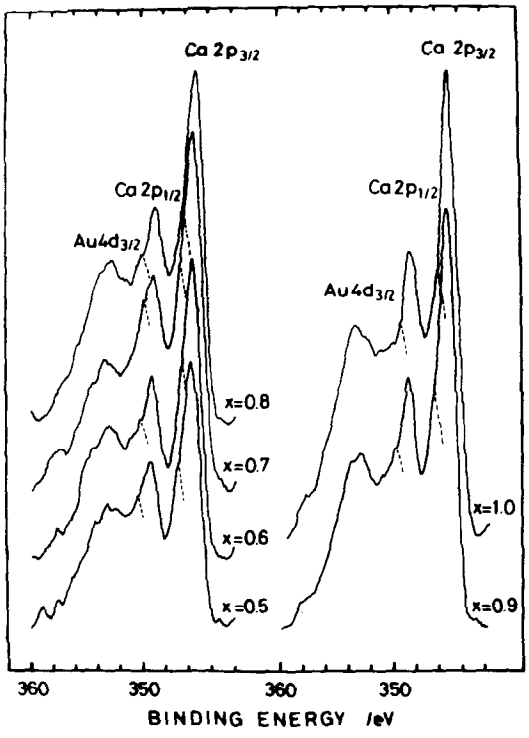

FIG. 2. XPS spectra of the Ca2p level in the system $(Nd_{1-x}Ca_x)MnO_{2.99}$.

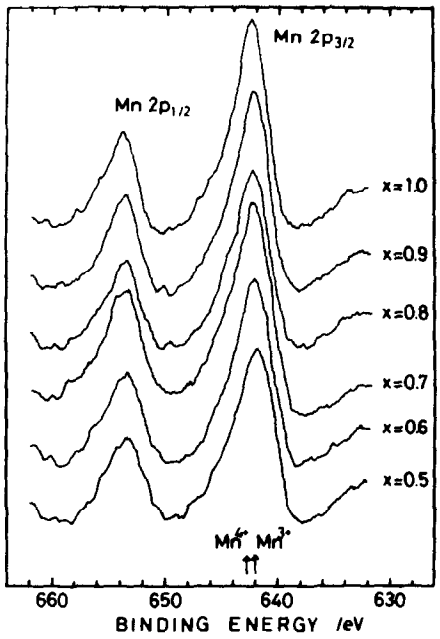

FIG. 3. XPS spectra of the Mn2p level in the system $(Nd_{1-x}Ca_x)MnO_{2.99}$.

Figure 3 shows the XPS spectra of the Mn2p level. Both the Mn2$p_{1/2}$ and Mn2$p_{3/2}$ peaks are broad. Both the integrated intensity and the binding energy of Mn2p are independent of the composition. The binding energy of Mn2$p_{3/2}$ in $LaMn^{3+}O_3$ and $Mn^{4+}O_2$ is ca. 642.0 and 624.4 eV, respectively (*9*, *10*). These values are also shown in Fig. 3. Kowalczyk *et al.* (*11*) reported that the Mn2$p_{3/2}$ peak in MnF_2 was broad and asymmetric toward the high binding energy site, and this asymmetry was discussed in terms of multiples splitting. From these results, the broad Mn2p peaks in $(Nd_{1-x}Ca_x)MnO_{2.99}$ are considered to be due to the mixed valency of both Mn^{3+} and Mn^{4+} ions and the multiplet structure in analogy with MnF_2.

The composition dependence of the binding energies of the Nd4d, Ca2p, Mn2p, and O1s peaks is shown in Fig. 4. The binding energy of Mn2p is independent of the com-

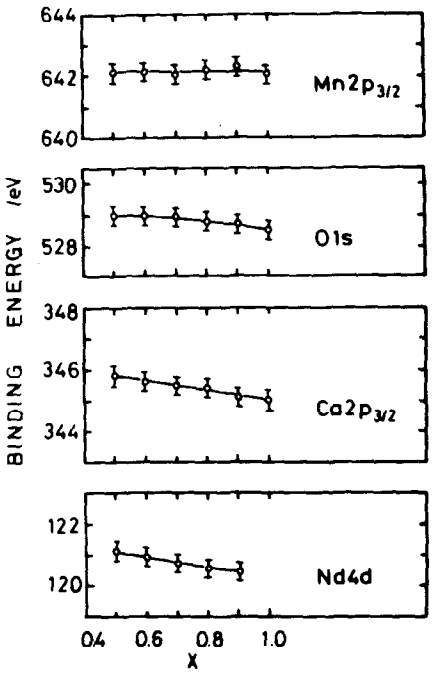

FIG. 4. The binding energy of Nd4*d*, Ca2*p*, Mn2*p*, and O1*s* levels vs composition in the system $(Nd_{1-x}Ca_x)MnO_{2.99}$.

position. On the other hand, the binding energies of Nd4*d*, Ca2*p*, and O1*s* decrease with increasing x. Carver *et al.* (*10*) discussed the relationship between the binding energy and the calculated charge on metal in the transition metal compounds. The charge on the metal in various compounds was calculated as follows (*12*). The calculated charge (q) on the metal equals the sum of the partial ionic character of the metal–ligand (L):

$$q = \sum_L I_L$$

I_L is related to the electronegativity difference between the bonded atoms by the Pauling equation (*13*):

$$I_L = 1 - \exp(-0.25(\chi_M - \chi_L)^2),$$

where χ_M and χ_L are the electronegativities of the metal and ligand, respectively.

According to the results reported by Carver *et al.* (*10*), the chemical shift of $Mn2p_{3/2}$ peak linearly increases with increasing calculated charge on Mn. As for the Ca and Nd compounds, the relationship between the chemical shift and the calculated charge on the metal have not been reported. The chemical shift and the calculated charge on Nd and Ca is shown in Fig. 5. In the present calculation, results both of the binding energy of Ca2*p* in Ca, CaO, $CaCO_3$, $CaSO_4$, $CaCl_2$, and CaF_2 reported by Wagner (*14*) and of the electronegativities of CO_3^{2-} and SO_4^{2-} reported by Huheey (*15*) are used. The chemical shift of $Ca2p_{3/2}$ linearly increases with increasing the calculated charge on Ca in analogy with $Mn2p_{3/2}$. On the other hand, there is little to report concerning the binding energy of the Nd compounds. We used the binding energy of Nd4*f* in Nd, Nd_2O_3, and NdF_3 (*16*) and that of Nd4*d* in Nd_2O_3 and $Nd_2(SO_4)_3$ (*17*). Although the number of Nd compounds

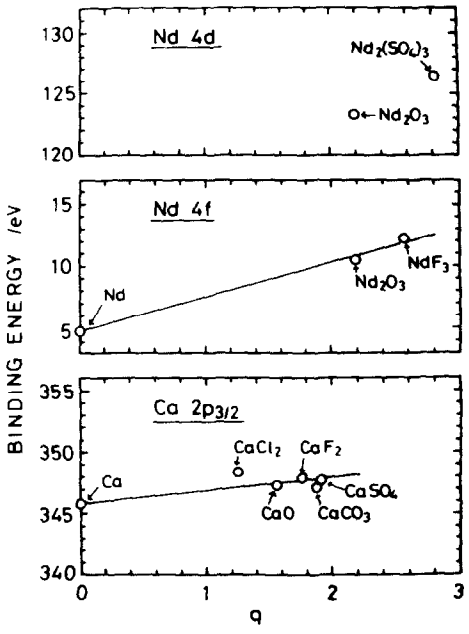

FIG. 5. The chemical shift of Nd4*d*, Nd4*f*, and Ca2*p* vs the calculated charge on Nd and Ca.

shown in Fig. 5 is little, it is expected that the chemical shift of the Nd peak linearly increases with increasing calculated charge on Nd.

According to the results reported by Haber *et al.* (*18*), the binding energy of the O1*s* peak in the transition metal oxides linearly decreases with increasing oxidation state of the transition metal. The decrease of the binding energy of the O1*s* peak shown in Fig. 4 is also explained by the increases of oxidation state of Mn. Since the calculated charge on Nd, Ca, and Mn equals the sum of the partial ionic character of the metal–ligand bonds as described previously, the present results on the composition dependence of the binding energy shown in Fig. 4 suggest that the constancy of the binding energy of the Mn2*p* peak is due to the invariance of the partial ionic character in Mn. On the other hand, the decrease of the binding energy of the Nd4*d* and Ca2*p* peaks is due to the decrease of the partial ionic character in Nd and Ca.

In the perovskite-type $(Nd_{1-x}Ca_x)MnO_{2.99}$ structure, two paths of the electron transfer are considered: One is Mn–O–Mn and the other is Mn–O–(Nd,Ca)–O–Mn. Takano *et al.* (*19*) reported that the electron transfer of the Mn–O–Sn path is dominant in the system $(Ca,Sr)Mn_{0.99}Sn_{0.01}O_3$ from Mössbauer measurement. From the results of XPS measurements of $(Nd_{1-x}Ca_x)MnO_{2.99}$, the partial ionic character of Mn is considered constant in the range $0.5 \leqq x \leqq 1.0$. Since the ionic character of both Ca and Nd is high in the Ca-poor region, the chemical bonding of (Nd,Ca)–O is ionic and it is difficult for the electron transfer of the Mn–O–(Nd,Ca)–O–Mn path to occur. The electron transfer of the Mn–O–Mn path is dominant in the Ca-poor region. With increasing x, the partial ionic character of both Nd and Ca decreases and the chemical bonding of (Nd,Ca)–O becomes covalent. The electron transfer of the Mn–O–(Nd,Ca)–O–Mn path occurs in analogy with that of the Mn–O–Mn path. However, in the high Ca-rich region, the covalency of the (Nd,Ca)–O bond decreases and the electron transfer of the Mn–O–(Nd,Ca)–O–Mn path is prevented with increasing x, because the electronegativity of Ca is larger than that of Nd (*20*). Consequently, the electrical resistivity has a minimum value at ca. $x = 0.9$.

In conclusion, the integrated intensity of Nd4*d* linearly decreases and that of Ca2*p* linearly increases with increasing x. The binding energies of Nd4*d*, Ca2*p*, and O1*s* decrease. Both the integrated intensity and the binding energy of Mn2*p* are independent of the composition. The variation of the binding energy is due to the partial ionic character of Nd and Ca. The decrease of O1*s* is due to an increase of the oxidation state of Mn. In the Ca-poor region, the electron transfer of the Mn–O–Mn path is dominant. With increasing x, the electron transfer of the Mn–O–(Nd,Ca)–O–Mn path also occurs. In a high Ca-rich region, the high electronegativity of Ca prevents the electron transfer of the Mn–O–(Nd,Ca)–O–Mn path. The electrical properties are strongly influenced by these paths of the electron transfer.

References

1. H. TAGUCHI, M. NAGAO, AND M. SHIMADA, *J. Solid State Chem.*, in press.
2. H. TAGUCHI AND M. SHIMADA, *J. Solid State Chem.* **63,** 290 (1986).
3. N. F. MOTT, "Metal–Insulator Transition," Taylor & Francis, London (1974).
4. V. JOSHI, O. PARKASH, G. N. RAO, AND C. N. R. RAO, *J. Chem. Soc., Faraday Trans. 2,* 75 (1979).
5. J. G. GOODENOUGH, *J. Appl. Phys.* **37,** 1415 (1966).
6. H. TAGUCHI AND M. SHIMADA, *Phys. Status Solidi B* **131,** K59 (1985).
7. H. TAGUCHI AND M. SHIMADA, *J. Solid State Chem.* **67,** 37 (1987).
8. N. MIZUTANI, N. OKUMA, A. KITAZAWA, AND M. KATO, *J. Chem. Soc. Japan, Ind. Chem.* **73,** 1103 (1970).
9. D. J. LAM, B. W. VEAL, AND D. E. ELLIS, *Phys. Rev. B* **22,** 5730 (1972).

10. J. CARVER, G. K. SCHWEITZER, AND T. A. CARLSON, *J. Chem. Phys.* **57,** 973 (1972).
11. S. P. KOWALCZYK, L. LEY, F. R. MCFEELY, AND D. A. SHIRLEY, *Phys. Rev. B* **11,** 1721 (1975).
12. W. B. HUGHES AND B. A. BALDWIN, *Inorg. Chem.* **13,** 1531 (1974).
13. L. PAULING, "The Nature of the Chemical Bond," 3rd ed., Cornell Univ. Press, New York (1960).
14. C. D. WAGNER, *in* "Practical Surface Analysis by Auger and X-Ray Photoelectron Spectroscopy," (D. Briggs and M. P. Seah, Eds.), Wiley, New York (1983).
15. J. E. HUHEEY, *J. Phys. Chem.* **70,** 2086 (1966).
16. P. A. COX, Y. BAER, AND C. K. JØRGENSEN, *Chem. Phys. Lett.* **22,** 433 (1973).
17. Y. UWAMINO, T. ISHIZUKA, AND H. YAMATERA, *J. Electron Spectrosc. Relat. Phenom.* **34,** 67 (1984).
18. J. HABER, J. STOCH, AND L. UNGIER, *J. Electron Spectrosc. Relat. Phenom.* **9,** 459 (1976).
19. M. TAKANO, Y. TAKEDA, M. SHIMADA, T. MATSUZAWA, T. SHINJO, AND T. TAKADA, *J. Phys. Soc. Japan* **39,** 656 (1975).
20. W. GORDY AND J. O., THOMAS, *J. Chem. Phys.* **24,** 439 (1956).